# Temperature Characteristics of Bilayer Thin-Film Devices Under Organic Interface Limited Current Conduction*

Yang Qingsen, Peng Yingquan†, Xing Hongwei, Li Xunshuan, Yuan Jianting, Ma Chaozhu, and Zhao Ming

(*School of Physical Science and Technology, Lanzhou University, Lanzhou* 730000, *China*)

**Abstract**: Temperature characteristics are important for the performance of organic thin film devices. On the basis of the hopping theory of Miller-Abrahams, an analytical model of charge transport for bilayer organic devices under the organic-organic interface limited current conduction is developed. The dependence of current, field, and carrier distribution in bilayer organic devices with the structure of "injection electrode/Layer Ⅰ/Layer Ⅱ/collection electrode" on temperature are numerically analyzed. We conclude that, for a given applied voltage, when temperature is raised, the voltage of Layer Ⅰ will increase, and the field will be higher. Meanwhile, the voltage of Layer Ⅱ will decrease, the field will become weaker accordingly, and the current of the device will increase.

**Keywords**: organic-organic interface limited; temperature characteristics; numerical analysis
**PACC**: 7280L
**CLC number**: TN304.50 **Document code**: A **Article ID**: 0253-4177(2008)06-1075-06

## 1 Introduction

The temperature characteristics of organic bilayer devices is of great importance for the understanding of organic thin film devices (OTFDs), like organic light-emitting devices[1~3] and organic photodetectors[4~6]. Current conduction in single layer OTFDs can be generally divided into two cases, namely the injection limited conduction and the bulk limited conduction. There are two limiting factors for current conduction in single layer devices. For single layer OTFDs with high injection energy barrier, high mobility, and small thickness, the current conduction is usually injection limited. The current is determined mainly by the injection barrier and the electric field, while the transport property (mobility, trap, thickness, and so on) of the organic have only a minor effect on the current density. For single layer OTFDs with lower carrier injection barrier, low mobility, and large thickness, the current conduction is bulk limited. The current is determined by the transport property of the organic bulk, while the injection barrier has only a minor effect on the current density.

For bilayer OTFDs, besides the metal-organic contact and the organic bulks, there is an additional limiting factor, namely the organic-organic interface. Bilayer OTFDs therefore have three current conducting states: the injection-limited, the bulk-limited, and the organic-organic (OO) interface limited current conduction. When the injection barrier is high, the organic layers are thin and their conductivities are high, and the energy barrier at the organic-organic interface is low, then the current conduction of the device is injection limited. When the organic layers are thick and high resistive, and the energy barrier at the metal-organic contact and at the organic-organic interface are low, then the current conduction of the device is bulk limited. When the energy barrier at the OO interface is high, the injection barrier at the metal-organic contact is low, and two organic layers are thin and conductive, then the current conduction in the bilayer device will be mainly limited by the energy barrier at the OO interface. We denote this kind of current conduction in bilayer devices as organic-organic interface limited (OOIL) conduction.

Although there are many research works concerning the modelling of multilayer organic devices[7~11], few reports about the temperature characteristics of distribution of current, field, and charges in bilayer devices have been seen. In this paper, we report the temperature characteristics at the distribution of electric field and carrier concentration in bilayer devices at OOIL current conduction.

* Project supported by the Natural Science Foundation of Gansu Province (No. ZS021-A25-003-Z)
† Corresponding author. Email: yqpeng@lzu.edu.cn
Received 29 November 2007, revised manuscript received 22 January 2008

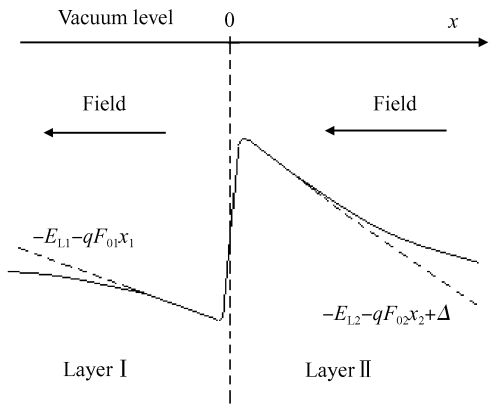


Fig. 1 Schematic diagram of potential distribution near the organic-organic interface

## 2 Numerical model

### 2.1 Charge transport across an organic-organic interface

Although tremendous research work has been done on carrier injection at metal-organic (MO) interfaces[12~16] and on electronic structure of OO interfaces[17~20], investigations on the carrier transport across OO interfaces are still very limited. Arkihipov *et al*.[21] have proposed an analytical model for carrier transport across the interface between two disordered organic semiconductors. Although the Schottky barrier, electric field, and hopping parameters of Layer Ⅱ (Fig. 1) are included in that model, the electric field in Layer Ⅰ and the carrier density in both layers are not included. Thus, the model is unsuitable for practical device modelling.

The basis for a traditional approach to the analysis of charge carrier kinetics in disordered hopping systems is the Miller-Abrahams expression[22] that determines the carrier jump rate from a starting transport site to a target transport site. We apply the Miller-Abrahams formalism to the hopping of electrons across the OO interface under the influence of an electric field. The hopping rate from a starting site located at $x_1$ in Layer Ⅰ to a target site located at $x_2$ in Layer Ⅱ is:

$$\nu_1(x_1 \to x_2) = \nu_{01}\exp\left[-2\gamma_1(x_2-x_1) - \frac{E_2(x_2)-E_1(x_1)+|E_2(x_2)-E_1(x_1)|}{2k_BT}\right] \quad (1)$$

where $\nu_{01}$ is the attempt-to-jump frequency, $\gamma_1$ the inverse localization radius of Layer Ⅰ, $k_B$ the Boltzmann constant, and $T$ the temperature. The zero point of the coordinate $x$ is located at the OO interface, so that $x_1$ is always smaller than or equal to zero, and $x_2$ greater than or equal to zero. In the vicinity of the interface, the potential energy $E_1(x_1)$ and $E_2(x_2)$ can be expressed as (Fig. 1)

$$E_1(x_1) = -E_{L1} - qF_{01}x_1 \quad (2)$$

$$E_2(x_2) = -E_{L2} - qF_{02}x_2 + \Delta \quad (3)$$

Here, $E_{L1}$ and $F_{01}$ are the LUMO energy of Layer Ⅰ, and the electric field near the OO interface on Layer Ⅰ side, respectively. $E_{L2}$ and $F_{02}$ are the LUMO energy and corresponding electric field of Layer Ⅱ, respectively. $q$ is elementary charge, and $\Delta$ is the energy offset or the vacuum-level shift of Layer Ⅱ in respect to the vacuum level of Layer Ⅰ caused by the interface dipole[23].

Let $n_1$ be the electron concentration in the vicinity of $x_1$ in Layer Ⅰ and $a_1$ the mean distance of the nearest transport sites (DNTS) to the OO interface in Layer Ⅰ, then the jump-rate density from Layer Ⅰ into the $i$-th transport site located at position $a_2+(i-1)b_2$ in Layer Ⅱ is:

$$\Psi_{1i} = \int_{-d_1}^{-a_1} \nu_1[x_1 \to a_2+(i-1)b_2]n_1(x_1)\mathrm{d}x_1 \quad (4)$$

where $d_1$ is the thickness of Layer Ⅰ. $a_2$ and $b_2$ are the mean DNTS and mean distance of transport sites in Layer Ⅱ. Substituting Eqs. (1)~(3) into Eq. (4), we obtain:

$$\Psi_{1i} = \frac{2\nu_{01}n_{01}k_BT}{qF_{01}} \times \exp\left\{-2\gamma_1\left[\left(1-\frac{F_{02}}{F_{01}}\right)(a_2+(i-1)b_2)+\frac{\phi+\Delta}{qF_{01}}\right]\right\} \times \int_{y_{10,i}}^{y_{1f,i}} \exp\left[\left(\frac{4\gamma_1k_BT}{qF_{01}}-1\right)y_1-|y_1|\right]\mathrm{d}y_1 \quad (5)$$

with

$$\phi = E_{L1} - E_{L2} \quad (6)$$

$$y_{10,i} = \frac{\phi+\Delta-qF_{02}[a_2+(i-1)b_2]-qF_{01}[a_1+(m_{s1}-1)b_1]}{2k_BT} \quad (7)$$

$$y_{1f,i} = \frac{\phi+\Delta-qF_{02}[a_2+(i-1)b_2]-qF_{01}a_1}{2k_BT} \quad (8)$$

$$m_{s1} = \frac{d_1-a_1}{b_1}+1 \quad (9)$$

The total jump-rate density from Layer Ⅰ into Layer Ⅱ is then:

$$\Psi_1 = \sum_{i=1}^{m_{s1}-1}\Psi_{1i} \quad (10)$$

Similarly, the jump-rate density from Layer Ⅱ into Layer Ⅰ is:

$$\Psi_2 = \sum_{i=1}^{m_{s2}-1}\Psi_{2i} \quad (11)$$

$$\Psi_{2i} = \frac{2\nu_{02}n_{02}k_BT}{qF_{02}} \times \exp\left\{-2\gamma_2\left[\left(1+\frac{F_{01}}{F_{02}}\right)(a_1+(i-1)b_1)+\frac{\phi+\Delta}{qF_{02}}\right]\right\}$$

$$\times \int_{y_{20,i}}^{y_{2f,i}} \exp\left[-\left(\frac{4\gamma_2 k_B T}{qF_{02}}+1\right)y_2 - |\ y_2\ |\right]\mathrm{d}y_2 \quad (12)$$

with

$$y_{20,i} = \frac{-\phi-\Delta-qF_{01}[a_1+(i-1)b_1]+qF_{02}a_2}{2k_B T} \quad (13)$$

$$y_{2f,i} = \frac{-\phi-\Delta-qF_{01}[a_1+(i-1)b_1]+qF_{02}[a_2+(m_{s2}-1)b_2]}{2k_B T} \quad (14)$$

$$m_{s2} = \frac{d_2-a_2}{b_2}+1 \quad (15)$$

The current density across the OO interface is then

$$J_{oo} = q(\Psi_1-\Psi_2) \quad (16)$$

### 2.2 Numerical model for OOIL current conduction in bilayer organic devices

At OOIL current conduction, charges will be accumulated in Layer Ⅰ due to the block of the energy barrier at the OO interface. Thus, both the drift and diffusion motion of the carrier should be considered. While in Layer Ⅱ, charges injected from Layer Ⅰ will be transported to the collecting electrode due the high conductivity of this layer. That is, the charge accumulation in Layer Ⅱ is weak, so that the diffusion component of the current can be neglected. The trap density in organic materials with high conductibility, such as Layer Ⅱ, is usually low and can be ignored.

There exist traps in most organic thin films due to structural disorder and impurities. The energy distribution due to structural disorder can be described by a Gaussian function, which can be approximated by an exponential function in the energy range concerned. We consider a bilayer single-carrier organic thin film device composed of a layer with exponentially distributed traps (Layer Ⅰ) and another which is trap free (Layer Ⅱ). The electric field $F_1$, total electron density $n_1$ and current density $j_{b1}$ at position $x_1$ in Layer Ⅰ are associated through the following equations (Fig. 1):

$$\frac{\mathrm{d}F_1}{\mathrm{d}x} = -\frac{qn_1}{\varepsilon_0\varepsilon_{r1}} \quad (17)$$

$$n_1 = n_{f1}+n_{t1} \quad (18)$$

$$j_{b1} = q\mu_1 n_{f1}F_1 - D_1 q\frac{\mathrm{d}n_{f1}}{\mathrm{d}x} \quad (19)$$

$$D_1 = \frac{\mu_1 k_B T}{q}\ \text{(Einstein relation)} \quad (20)$$

Here, $\varepsilon_0$ and $\varepsilon_{r1}$ are the permittivity of a vacuum and the relative dielectric constant of Layer Ⅰ respectively; $n_{f1}$, $n_{t1}$ and $n_1$ are the free electron, trapped electron, and total electron concentrations, respectively. $\mu_1$ is electron mobility and $D_1$ the electron diffusion coefficient; $k_B$ and $T$ are the Boltzmann constant and ambient temperature, respectively. The zero point of coordinate $x$ is located at the OO interface.

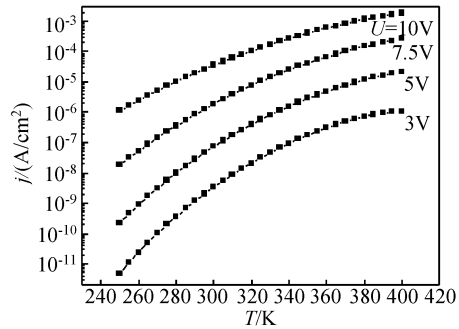


Fig. 2　Calculated dependence of current density on temperature　The parameters used are $H_{tp1}=5\times10^{17}\,\mathrm{cm}^{-3}$, $l_{p1}=6$, $d_1=100\,\mathrm{nm}$, $d_2=100\,\mathrm{nm}$, $\mu_1=10^{-4}\,\mathrm{cm}^2/(\mathrm{V}\cdot\mathrm{s})$, $\mu_2=10^{-3}\,\mathrm{cm}^2/(\mathrm{V}\cdot\mathrm{s})$, $\varepsilon_{r2}=2$, $\nu_{01}=10^{14}\,\mathrm{s}^{-1}$, $\gamma_1=2$, $a_1=1$, $a_2=1$, $\Delta=0$, $\varphi=0.5\,\mathrm{eV}$.

The density of free electrons in Layer Ⅰ, $n_{f1}$, is related to the total electron concentration through the following equation[24]:

$$n_{f1} = N_{01}\left(\frac{\sin\left(\frac{\pi}{l_1}\right)}{H_{t1}\left(\frac{\pi}{l_1}\right)}\right)n_1^{l_1} \quad (21)$$

where $l_1$ is the relative trap depth of exponentially distributed traps[8~10,25,26], and $H_{t1}$ is the total trap density.

From electric field $F_1$, the voltage drop in Layer Ⅰ, $U_1$ can be calculated:

$$U_1 = \int_{-d_1}^{0} F_1(x)\mathrm{d}x \quad (22)$$

As no accumulation of charges occurs in Layer Ⅱ, the carry density and electric field are uniformly distributed over the entire layer. The current density $j_{b2}$, carry density $n_2$, and electric field $F_2$ in Layer Ⅱ can be described by the following equation:

$$j_{b2} = q\mu_2 n_2 F_2 \quad (23)$$

$$F_2 = F_{02} = \frac{U_2}{d_2} \quad (24)$$

From current continuity, we obtain:

$$j_{b1} = j_{oo} = j_{b2} = j \quad (25)$$

$$U = U_1+U_2 \quad (26)$$

Equations (5)～(26) were solved for the distribution of the field and carrier concentration, using standard numerical methods.

## 3 Results and discussion

Figure 2 shows the dependence of current density on the temperature under different voltages. The current increases gradually as the temperature increases.

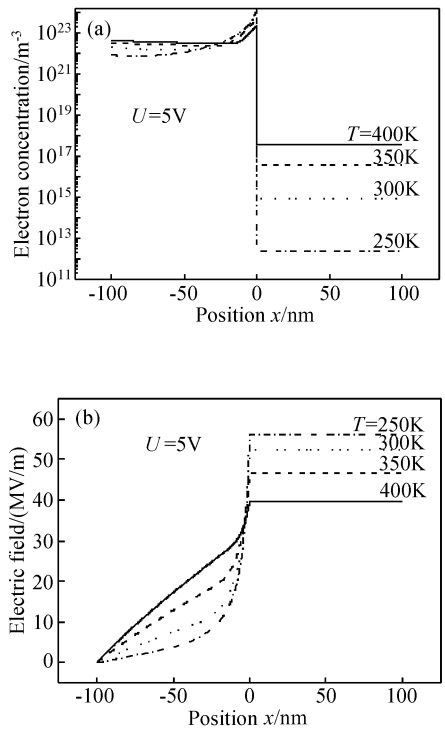


Fig. 3 Distribution of the electric field and carrier concentration for different temperatures (a) Distribution of carrier concentration; (b) Electric field distribution The parameters used are $H_{tp1}=5\times10^{17}\,cm^{-3}$, $l_{p1}=6$, $d_1=100nm$, $d_2=100nm$, $\mu_1=10^{-4}cm^2/(V\cdot s)$, $\mu_2=10^{-3}cm^2/(V\cdot s)$, $\varepsilon_{r2}=2$, $\nu_{01}=10^{14}s^{-1}$, $\gamma_1=2$, $a_1=1$, $a_2=1$, $\Delta=0$, $\varphi=0.5eV$.

According to Eq. (1), when the temperature increases, the hopping rate becomes greater, that is, carriers can transport across the OO interface more easily as the temperature increases.

Figure 3 shows the distribution of electron concentration and electric field at different temperatures for an operation voltage of 5V. Figure 3(a) shows that the electron concentration increases as the temperature increases, and the electron concentration near the OO interface on Layer Ⅰ side increases slowly, while the electron concentration near the OO interface on Layer Ⅱ side increases rapidly. When the temperature is high, according to Eq. (1), carriers can transport across the OO interface more easily. So more carriers can transport across the barrier into Layer Ⅱ when the electron concentration is high in Layer Ⅰ, which results in a more rapid increase of carrier concentration in Layer Ⅱ.

When the total voltage of the device is held constant, the ratio of mean electron concentration in Layer Ⅰ to the electron concentration in Layer Ⅱ becomes smaller as the temperature increases. On the other hand, the ratio of the resistance of Layer Ⅰ to Layer Ⅱ increases, changing the distribution of the voltage in Layer Ⅰ and Layer Ⅱ: the voltage of Layer Ⅰ increases, and that of Layer Ⅱ decreases. So, when the temperature increases, the electric field in Layer Ⅰ increases, while the field in Layer Ⅱ decreases. (Fig. 3(b))

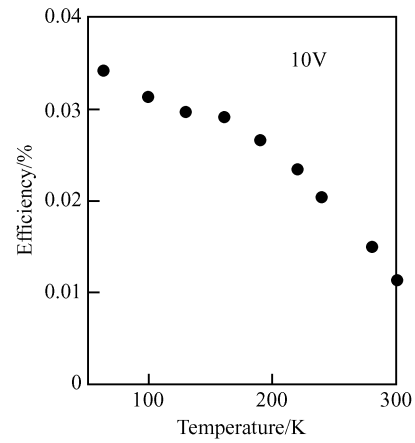


Fig. 4 Measured dependence of luminescence efficiency on the temperature of the device "Al/$Alq_3$/TPD/ITO" from Ref. [27]

Saha *et al.*'s study[27] on the organic light-emitting devices (OLEDs) with a structure of Al/ tris-(8-hydroxy) quinoline aluminum($Alq_3$)/ N,N'-diphenyl-N,N'bis(3-methylphenyl)-[1-1'-biphenyl]-4-4'-diamine(TPD)/ITO concluded that the luminescence efficiency decreases as the device temperature increases (Fig. 4), which can be explained by this model. The LUMO and HOMO energy of $Alq_3$ are 3.3 and 6.0eV, respectively[28]. The LUMO and HOMO energy of TPD are 2.4 and 5.5eV, respectively[29]. Thus, under normal work conditions (ITO as anode, Al as cathode), the electron transport barrier at $Alq_3$/TPD interface is large (0.9eV), so the electrons injected from the Al electrode accumulate near the OO interface on the $Alq_3$ side, as in Layer Ⅰ in this model. The majority of holes injected from the ITO electrode into the TPD layer transport across the OO interface into the $Alq_3$ layer, and recombine radiatively with electrons there. A small number of electrons transport across the OO interface and recombine with holes in the TPD layer nonradiatively, so there is no electron accumulation in the TPD layer, as in Layer Ⅱ in our model. So, the conduction of electron current in this device can be considered as OOIL conduction due to the thin $Alq_3$ layer and the large electron transport barrier at the OO interface. According to Fig. 2, for a given voltage, the ratio of the electron current from $Alq_3$ to TPD to the total current becomes greater when the temperature increases. As the temperature increases, the nonradiative recombination in TPD increases, which leads to a decrease in luminescence efficiency.

## 4 Conclusion

Based on the Miller-Abrahams theory, a numerical model for charge transport at OO interfaces is established. The dependences of current density, distribution of field, and electron concentration on temperature under OOIL current conduction are analysed. The results show that: (1) the higher the temperature of the device, the larger the current, (2) carrier concentrations in Layer Ⅰ and Layer Ⅱ increase with temperature, and carrier concentration in Layer Ⅱ increases more rapidly than in Layer, and (3) the change of temperature influences the distribution of voltage in Layer Ⅰ and Layer Ⅱ. For a given voltage, when the temperature increases, the voltage and the electric field of Layer Ⅰ increase, while the voltage and the electric field of Layer Ⅱ decrease.

### References


[1] Hsiao C C, Chang C H, Jen T H, et al. High-efficiency polymer light-emitting diodes based on ploy[2-methoxy-5-(2-ethylhexyloxy)-1, 4-phenylene vinylene] with plasma-polymerized $CHF_3$-modified indium tin oxide as an anode. Appl Phys Lett, 2006, 88(3): 033512

[2] Tang C W, VanSlyke S A. Organic electroluminescent diodes. Appl Phys Lett, 1987, 51(12): 913

[3] Zheng Daishun, Zhang Xu, Qian Keyuan. Influence of hole buffer layer CuPc on properties of organic light-emitting devices. Chinese Journal of Semiconductors, 2005, 26(1): 78 (in Chinese) [郑代顺, 张旭, 钱可元. 空穴缓冲层 CuPc 对有机电致发光器件特性的影响. 半导体学报, 2005, 26(1): 78]

[4] Lin H W, Ku S Y, Huang C W, et al. Highly efficient visible-blind organic ultraviolet photodetectors. Adv Mater, 2005, 17(20): 2489

[5] Xue J G, Forrest S R. Carrier transport in multilayer organic photodetectors: I. Effects of layer structure on dark current and photoresponse. J Appl Phys, 2004, 95(4): 1859

[6] Xue J G, Forrest S R. Carrier transport in multilayer organic photodetectors: II. Effects of anode preparation. J Appl Phys, 2004, 95(4): 1869

[7] Zhang J, Wang J, Wang H B. Organic thin-film transistors in sandwich configuration. Appl Phys Lett, 2004, 84(1): 142

[8] Peng Y Q, Zhang F J, Song C A. Numerical investigations on the current conduction in bilayer organic light-emitting devices with ohmic injection of charge carriers. Chinese Physics, 2003, 12(7): 796

[9] Peng Y Q, Song C A, Sun S. Numerical model for current conduction in single layer organic light-emitting devices including both bulk and injection effects. Semicod Sci Technol, 2004, 19: 1117

[10] Peng Y Q, Zhang L, Zhang X. Numerical study of optimization of layer thickness in bilayer organic light-emitting diodes. Chinese Journal of Semiconductors, 2003, 24(5): 454

[11] Nikitenko V, Bässler H. An analytic model of electroluminescence in bilayer organic light emitting diodes with ohmic injection of charge carriers. J Appl Phys, 2001, 90(4): 1823

[12] Hu W P, Nakashima H, Furukawa K. Carrier injection from gold electrodes into thioacetyl-end-functionalized poly(para-phenyleneethynylene)s. Phys Rev B, 2004, 69(16): 165207

[13] Scott J C, Malliaras G G. Charge injection and recombination at the metal-organic interface. Chem Phys Lett, 1999, 299: 115

[14] Peng Y Q, Lu F P. Injection of holes at indium tin oxide/dendrimer interface: An explanation with new theory of thermionic emission at metal/organic interface. Appl Surf Sci, 2006, 252: 6275

[15] Koch N, Duhm S, Rabe J P. Optimized hole injection with strong electron acceptors at organic-metal interfaces. Phys Rev Lett, 2005, 95(23): 237601

[16] Peng Y Q, Yang J H, Sun S. Numerical study on the optimization of hole injection layers in organic light-emitting devices. Semicond Sci Technol, 2005, 20: 221

[17] Gao W Y, Kahn A. Effect of electrical doping on molecular level alignment at organic-organic heterojunctions. Appl Phys Lett, 2003, 82(26): 4815

[18] Rajagopal A, Wu C I, Kahn A. Energy level offset at organic semiconductor heterojunctions. J Appl Phys, 1998, 83(5): 2649

[19] Braun S, Osikowicz W, Wang Y, et al. Energy level alignment regimes at hybrid organic-organic and inorganic-organic interfaces. Organic electronics, 2007, 8: 14

[20] Kampen T U. Electronic structure of organic interfaces-a case study on perylene derivatives. Appl Phys A, 2006, 82: 457

[21] Arikhipov V I, Emelianova E V, Bässler H. Charge carrier transport and recombination at the interface between disordered organic dielectrics. J Appl Phys, 2001, 90(5): 2352

[22] Miller A, Abrahams E. Impurity conduction at low concentrations. Phys Rev, 1960, 120(3): 745

[23] Lau K M, Tang J X, Sun H Y. Interfacial electronic structure of copper phthalocyanine and copper hexadecafluorophthalocyanine studied by photoemission. Appl Phys Lett, 2006, 88(17): 173513

[24] Bonham J S, Jarvis D H. A new approach to space-charge-limited conduction theory. Austr J Chem, 1977, 30: 705

[25] Peng Y Q, Zhang F J, Tai X S, et al. Numerical analysis of the mechanism of carrier transport in organic light-emitting devices. Chinese Physics, 2002, 11(10): 1076

[26] Peng Y Q, Zhang F J, Zhang X, et al. Numerical study of the current conduction in single-layer organic light-emitting devices. Appl Phys A, 2004, 78: 369

[27] Saha S K, Su Y K, Juang F S. Temperature- and field-dependent quantum efficiency in tris-(8-hydroxy) quinoline aluminum light-emitting diodes. J Appl Phys, 2001, 89(12): 8175

[28] Ikai M, Tokito S, Sakamoto Y, et al. Highly efficient phosphorescence from organic light-emitting devices with an exciton-block layer. Appl Phys Lett, 2001, 79(2): 156

[29] Kawabe Y, Abe J. Electron mobility measurement using exciplex-type organic light-emitting diodes. Appl Phys Lett, 2002, 81(3): 493

# 有机双层薄膜器件界面限制传导温度特性研究*

杨青森 彭应全† 邢宏伟 李训栓 袁建挺 马朝柱 赵 明

（兰州大学物理科学与技术学院，兰州 730000）

**摘要**：通过对器件的温度特性的研究，能够使器件在合适的温度下保持稳定的工作状态.本文以 Miller-Abrahams 跳跃传导理论为基础，建立了有机-有机界面限制电流传导的电荷传输的解析模型.依据此模型分析了结构为“注入电极/有机层Ⅰ/有机层Ⅱ/收集电极”的双层薄膜器件在有机界面限制电流传导状态下的电流、电场和载流子分布与工作温度的变化关系.结果表明，在给定的工作电压下，温度升高时降落在层Ⅰ的电压升高，电场增强，而降落在层Ⅱ的电压降低，电场减弱，同时器件的电流增大.

**关键词**：有机-有机界面限制；温度特性；数值分析

**PACC**：7280L

**中图分类号**：TN304.50 **文献标识码**：A **文章编号**：0253-4177(2008)06-1075-06

* 甘肃省自然科学基金资助项目(批准号：ZS021-A25-003-Z)

† 通信作者.Email：yqpeng@lzu.edu.cn

2007-11-29 收到，2008-01-22 定稿